Letter

# Hund bands in spectra of multiorbital systems

M. Środa,[1] J. Mravlje,[2] G. Alvarez,[3] E. Dagotto,[4,5] and J. Herbrych[1]

[1]*Institute of Theoretical Physics, Faculty of Fundamental Problems of Technology, Wrocław University of Science and Technology, 50-370 Wrocław, Poland*

[2]*Jožef Stefan Institute, SI-1000 Ljubljana, Slovenia*

[3]*Computational Sciences and Engineering Division, Oak Ridge National Laboratory, Oak Ridge, Tennessee 37831, USA*

[4]*Department of Physics and Astronomy, University of Tennessee, Knoxville, Tennessee 37996, USA*

[5]*Materials Science and Technology Division, Oak Ridge National Laboratory, Oak Ridge, Tennessee 37831, USA*

(Received 20 October 2022; revised 16 March 2023; accepted 11 July 2023; published 3 August 2023)

Spectroscopy experiments are routinely used to characterize the behavior of strongly correlated systems. An in-depth understanding of the different spectral features is thus essential. Here, we show that the spectrum of the multiorbital Hubbard model exhibits unique Hund bands that occur at energies given only by the Hund coupling $J_{\mathrm{H}}$, as distinct from the Hubbard satellites following the interaction $U$. We focus on experimentally relevant single-particle and optical spectra that we calculate for a model related to iron chalcogenide ladders. The calculations are performed via the density-matrix renormalization group and Lanczos methods. The generality of the implications is verified by considering a generic multiorbital model within dynamical mean-field theory.

DOI: 10.1103/PhysRevB.108.L081102

*Introduction.* Strongly correlated systems are at the heart of modern condensed matter physics. The celebrated single-band Hubbard model, describing (doped) Mott insulators, is still extensively studied in the context of Cu-based high-temperature superconductivity [1–3]. An equally exciting case is that of iron-based superconductors where the presence of several active orbitals leads to novel effects beyond the "standard" Mott physics [4–6]. A nontrivial example is the orbital-selective Mott phase (OSMP) [5,7–10], where Mott-localized and itinerant electrons coexist.

A key probe of electronic excitations is the single-particle spectral function $A(k, \omega)$, characterizing the excitations' dispersion. It is experimentally accessible by angle-resolved photoemission spectroscopy (ARPES) [11,12]. To understand the origin of different spectral features, it is convenient to consider idealized models that can be studied theoretically and monitor how the signatures of correlations (e.g., the Hubbard bands) evolve with increasing Coulomb interaction $U$. This is especially true for quantum systems of reduced dimensionality, for which quasiexact numerical methods [13,14], or even closed analytical solutions [15], provide unbiased information on the elementary excitations. However, even in reduced dimensionality obtaining accurate results for the multiorbital Hubbard model remains challenging. The difficulty lies in the exceptionally large Hilbert space. Because of that, the spectral functions are often calculated using the dynamical mean-field theory (DMFT) [16–19]. This approach, which strictly applies at large dimensionality, avoids the finite-size limitation, but often relies on solvers in Matsubara frequencies and hence the resulting spectral functions are blurred due to analytical continuation (see Ref. [20], which discusses this and introduces a method to alleviate the problem).

In this Letter, we numerically investigate the spectral functions of several multiorbital models. Our main result is summarized in Fig. 1(a). The electronic spectrum of a single-orbital model (without the Hund coupling $J_{\mathrm{H}} \to 0$) consists of the usual upper and lower Hubbard bands (UHB and LHB, respectively) that develop with $U$. In multiorbital systems, the finite $J_{\mathrm{H}}$ gives rise to additional excitations. Some of these states can appear at energies between UHB and LHB that depend exclusively on $J_{\mathrm{H}}$ (i.e., are independent of $U$), paving the way to measure $J_{\mathrm{H}}$ directly. Since such excitations occur due to the Hund coupling and have a robust dispersion [see Figs. 1(b) and 1(c) and Ref. [21] for the full spectrum of $A(k, \omega)$], we call them *Hund bands*. We recognize that the Hund bands arise whenever single-particle removal/addition processes yield a higher multiplet of the dominant valence subspace. This can occur provided (i) the higher multiplets exist, (ii) these multiplets are allowed by the selection rules upon adding/removing a particle, and (iii) the charge fluctuations are significant. All these requirements are met for Hund's metals. Earlier work documented multiplet splittings in the Hubbard bands [20,31,32], in the fully occupied orbital [33], found additional "holon-doublon" peaks [34–39], and analyzed the energy-level structure, revealing multiplets that violate the Hund's rules [40]. Here, we stress that charge excitations independent of $U$ are a *generic* consequence of the multiorbital systems.

To reach these conclusions, we use the density-matrix renormalization group method (DMRG) [41–46] and Lanczos diagonalization [2,47]. To show that our findings are generic, we study both the two- and three-orbital Hubbard model. Furthermore, we supplement our analysis with the effective model of the OSMP—the generalized Kondo-Heisenberg Hamiltonian. Finally, we confirm our findings with DMFT calculations. Our results apply to many experiments investigating the spectral properties of multiorbital materials, particularly iron-based compounds [48,49], ruthenates [33,50–52], iridates [53,54], and nickel oxides [55–59].

 

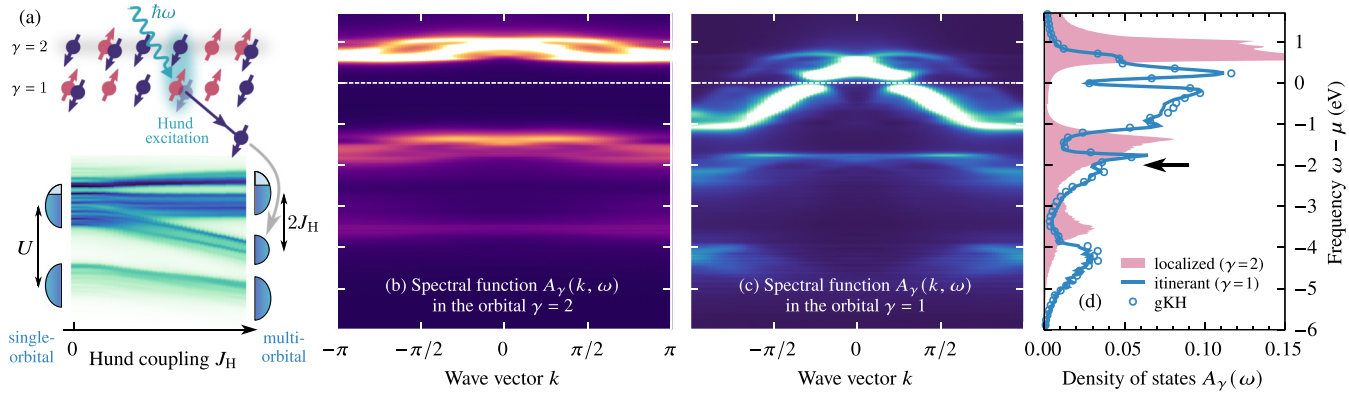


FIG. 1. (a) Sketch of the Hund band accompanying the standard Hubbard bands. (b), (c) Orbital- and momentum-resolved spectral function $A_\gamma(k, \omega)$ in the two-orbital Hubbard model for $n = 2.5$, $U/W = 1.3$, $J_H/U = 0.25$, $L = 48$ sites, and orbitals (b) $\gamma = 2$ and (c) $\gamma = 1$. The horizontal line marks the chemical potential $\mu$. (d) Orbital-resolved density of states $A_\gamma(\omega)$. Points depict the corresponding effective generalized Kondo-Heisenberg model (gKH); see the text for details. The arrow points at the Hund band in the itinerant orbital. Results obtained with DMRG using broadening $\eta = 0.04$.

*Model.* We focus on the SU(2)-symmetric multiorbital Hubbard-Kanamori chain,

$$\begin{aligned} H_H = &-\sum_{\gamma\gamma'\ell\sigma} t_{\gamma\gamma'}(c^\dagger_{\gamma\ell\sigma}c_{\gamma'\ell+1\sigma} + \text{H.c.}) + \sum_{\gamma\ell}\Delta_\gamma n_{\gamma\ell} \\ &+ U\sum_{\gamma\ell} n_{\gamma\ell\uparrow}n_{\gamma\ell\downarrow} + (U - 5J_H/2)\sum_{\gamma<\gamma',\ell} n_{\gamma\ell}n_{\gamma'\ell} \\ &- 2J_H\sum_{\gamma<\gamma',\ell}\mathbf{S}_{\gamma\ell}\cdot\mathbf{S}_{\gamma'\ell} + J_H\sum_{\gamma<\gamma',\ell}(P^\dagger_{\gamma\ell}P_{\gamma'\ell} + \text{H.c.}). \end{aligned} \quad (1)$$

Here, $c^\dagger_{\gamma\ell\sigma}$ creates an electron with spin $\sigma$ at orbital $\gamma$ of site $\ell$. $t_{\gamma\gamma'}$ is the symmetric hopping matrix in orbital space. $\Delta_\gamma$ denotes the crystal-field splitting. $n_{\gamma\ell} = \sum_\sigma n_{\gamma\ell\sigma}$ represents the total density of electrons. $U$ is the standard repulsive Hubbard interaction. $J_H$ is the Hund coupling between spins $\mathbf{S}_{\gamma\ell}$ at different orbitals $\gamma$. The last term $P^\dagger_{\gamma\ell}P_{\gamma'\ell}$ denotes interorbital pair hopping, $P_{\gamma\ell} = c_{\gamma\ell\uparrow}c_{\gamma\ell\downarrow}$. We assume open boundary conditions, as required by DMRG. For the two-orbital model, $\gamma \in \{1, 2\}$, we used (in eV) $t_{11} = -0.5$, $t_{22} = -0.15$, $t_{12} = t_{21} = 0$, $\Delta_1 = 0$, $\Delta_2 = 0.8$; whereas for the three-orbital model: $\gamma \in \{0, 1, 2\}$, $t_{00} = t_{11} = -0.5$, $t_{22} = -0.15$, $t_{02} = t_{12} = 0.1$, $t_{01} = 0$, $\Delta_0 = -0.1$, $\Delta_1 = 0$, $\Delta_2 = 0.8$. These values were previously used to study the iron-based ladders of the 123 family [9,10,60–63]. The bandwidth of the two-orbital model, $W = 2.1$, is used as the energy unit [64]. All energy labels given throughout the text are independent of the $J_H/U$ ratio.

We also study the minimal model of the OSMP: The generalized Kondo-Heisenberg model (gKH). This model was derived [10,62,63] to capture the static and dynamic properties of $BaFe_2Se_3$ iron-based ladder [65–67]. It describes interacting itinerant electrons (with spin $\mathbf{s}_i$) coupled via Hund coupling to the localized spins $\mathbf{S}_l$,

$$\begin{aligned} H_K = &-t_i\sum_{\ell\sigma}(c^\dagger_{\ell\sigma}c_{\ell+1\sigma} + \text{H.c.}) + U\sum_\ell n_{\ell\uparrow}n_{\ell\downarrow} \\ &+ K\sum_\ell \mathbf{S}_{l\ell}\cdot\mathbf{S}_{l\ell+1} - 2J_H\sum_\ell \mathbf{s}_{i\ell}\cdot\mathbf{S}_{l\ell}. \end{aligned} \quad (2)$$

For the gKH model, $t_i = -0.5$, $K = 4t_l^2/U$, $t_l = -0.15$, matching the OSMP of our two-orbital Hubbard model [10].

*Hund bands.* Let us study the orbital-resolved single-particle spectral function $A_\gamma(k, \omega)$ and the density of states (DOS) $A_\gamma(\omega) \propto \sum_\sigma(\langle\langle c^\dagger_{\gamma,L/2,\sigma}; c_{\gamma,L/2,\sigma}\rangle\rangle^h_\omega + \langle\langle c_{\gamma,L/2,\sigma}; c^\dagger_{\gamma,L/2,\sigma}\rangle\rangle^e_\omega)$ [21]. Here, $k$ is the momentum, $\omega$ the energy, and $\langle\langle\ldots\rangle\rangle^{h,e}_\omega$ represent the hole and electron components.

The origin of the Hund bands can be clearly illustrated in an OSMP system. Figures 1(b)–1(d) present data for the two-orbital Hubbard model (2oH) at electron filling $n = 2.5$ and interaction $U \simeq W$. Clearly, the narrow orbital $\gamma = 2$ [Fig. 1(b)] has a gap at the Fermi level $\mu$, while the orbital $\gamma = 1$ [Fig. 1(c)] is metallic with a finite DOS at $\mu$ (or a narrow pseudogap-like feature originating in the magnetic order [68]). This behavior is consistent with the OSMP [10]; the narrow orbital is Mott localized with the electron density equal to 1. However, instead of two excitation bands (UHB and LHB), expected from the Mott physics, we observe a prominent three-peak structure [see also the DOS in Fig. 1(d)]. This structure is also visible in the itinerant orbital ($\gamma = 1$), Fig. 1(c), with an electron density equal to 1.5. Note that the itinerant orbital's spectrum is accurately reproduced by the effective gKH model.

Let us take a closer look at how the three-peak spectrum develops with the interaction $U$. Figure 2(a) shows $A_1(\omega)$ for the gKH model at noninteger filling $n = 1.5$. In the $U \to 0$ limit, we recover the noninteracting behavior: A single metallic band. However, already at $U/W \simeq 0.8$, i.e., close to the OSMP transition [9,10], the three-peak structure is visible in $A_1(\omega)$, and becomes clearer the larger the interaction $U$ becomes. Since the three-peak structure is most pronounced for $U \gg W$, it is instructive to examine the atomic limit $U, J_H \to \infty$ of the gKH model; see Fig. 2(b). The atom realizes the noninteger filling $n = 1.5$ provided the ground states (gs) of the 1- and 2-electron subspaces are degenerate, which is achieved at $\mu = U + J_H/2$. Then, the gs consists of a local interorbital triplet, denoted as $|\text{T}\rangle$, which is degenerate with an itinerant doublon with localized spin, denoted as $|\text{D}\rangle$. By

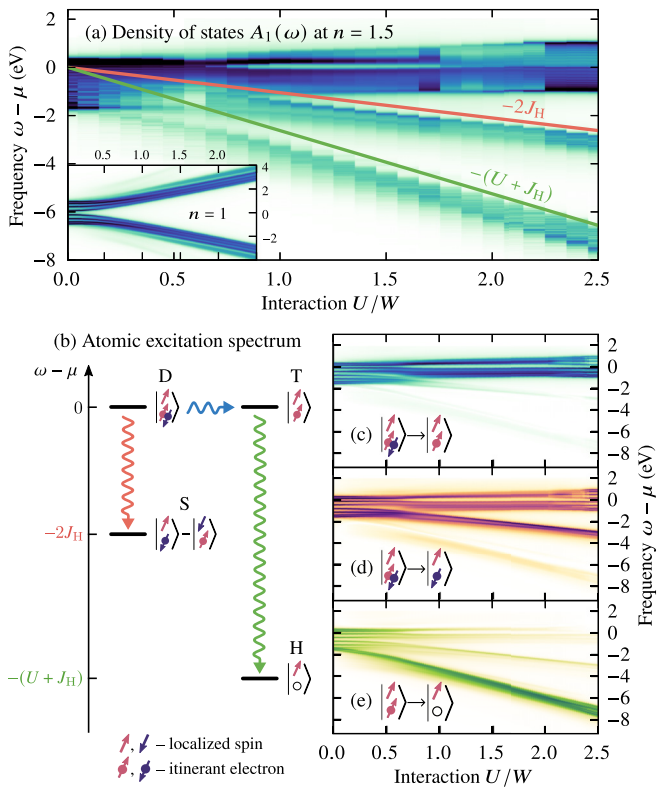


FIG. 2. (a) Interaction $U$ dependence of the itinerant orbital's density of states (DOS) $A_1(\omega)$ obtained for the gKH model with $L = 48$ sites, $J_H/U = 0.25$, and $n = 1.5$. Results obtained with DMRG using $\eta = 0.04$ broadening. The solid lines represent the atomic-limit transitions. Inset depicts the results for half electron filling $n = 1$. (b) Atomic excitation spectrum. For clarity, we mark only the hole-like (electron removal) excitations and show only one spin projection. D, T, S, H labels stand for doublon, triplet, singlet, and holon, respectively. (c)–(e) DOS $A_1(\omega)$ projected on the specific final configurations: (c) parallel spins, (d) antiparallel spins, and (e) on the holon; see the text for details. Results obtained with Lanczos diagonalization of $L = 8$ lattice with broadening $\eta = 0.05$.

removing an electron from the triplet, one creates a holon in the itinerant orbital ($|\mathrm{T}\rangle \to |\mathrm{H}\rangle$), with the cost of energy $U + J_H$. Interestingly, from the doubly occupied state, one can remove an electron in two different ways. Depending on the spin projection of the removed electron, one can arrive at a local triplet or singlet, $|\mathrm{D}\rangle \to |\mathrm{T}\rangle$ or $|\mathrm{D}\rangle \to |\mathrm{S}\rangle$, respectively. The former is a zero-energy transition between degenerate states of the gs, while the latter costs an energy $2J_H$ as it breaks the Hund's rule. In Fig. 2(a), we plot the relevant energy scales of the atomic limit ($U + J_H$ and $2J_H$) and find good agreement with the full many-body calculations of the gKH chain.

*Projections on the atomic configurations.* To make a stronger case for the atomic-limit interpretation of the three-peak spectrum, we decompose the spectral function of the full many-body calculation into individual transitions [38]. To this end, we use the projector $\mathcal{P}$ onto specific configurations of the on-site Ising basis $|\gamma = 1, \gamma = 2\rangle$, i.e., $\langle\langle c^\dagger_{\gamma,L/2,\sigma}; \mathcal{P} c_{\gamma,L/2,\sigma}\rangle\rangle^{\mathrm{h}}_{\omega}$ [21]. For clarity, we discuss only the hole part (below $\mu$), as the electron part can be described analogously. Upon removing an electron from the itinerant orbital, we distinguish three contributions. (i) In Fig. 2(c), we project onto the parallel-spin configuration, $\mathcal{P} = |\uparrow,\uparrow\rangle\langle\uparrow,\uparrow| + |\downarrow,\downarrow\rangle\langle\downarrow,\downarrow|$. The resulting weight forms a band of excitations close to the Fermi level $\omega \simeq \mu$. This transition is responsible for the metallic properties of the lattice. (ii) In Fig. 2(d), we instead project onto the antiparallel configuration, $\mathcal{P} = |\uparrow,\downarrow\rangle\langle\uparrow,\downarrow| + |\downarrow,\uparrow\rangle\langle\downarrow,\uparrow|$. We observe large weight in the middle band and some smaller weight at $\omega \simeq \mu$. The middle band represents the interorbital singlet which breaks the Hund's rule: This is the $2J_H$ Hund excitation. The band at $\omega \simeq \mu$ represents the $S^z = 0$ component of the triplet ($|\uparrow,\downarrow\rangle + |\downarrow,\uparrow\rangle$), costing zero energy to excite. (iii) Finally, in Fig. 2(e), we project onto the holon configuration, $\mathcal{P} = |0,\uparrow\rangle\langle 0,\uparrow| + |0,\downarrow\rangle\langle 0,\downarrow|$. This gives the energetically lowest band of excitations, which we recognize as the LHB, arising from triplet to holon transitions. The starting state needs to be a triplet because singlets are excluded from the gs by the Hund's rule.

*Noninteger vs integer filling.* As shown above, for noninteger filling (doped system), the atomic limit is enough to explain the Hund bands. When the atomic gs of adjacent particle-number subspaces, say $N$ and $N - 1$, are degenerate, there is no cost $U$ for the transition from the gs of subspace $N$ to the gs of subspace $N - 1$. The excitation cost is zero; it is compensated by $\mu$ which is tuned to cause the degeneracy. However, if the $N - 1$ subspace contains not only the gs but also higher multiplets, these multiplets can be accessed in the photoemission process $N \to N - 1$ with just the energy $\propto J_H$. Analogous reasoning applies to inverse transitions $N - 1 \to N$. Thus, remarkably, this results in $U$-independent Hund bands.

Consider now this behavior in a more general system, hosting more atomic configurations with different $n$. In Fig. 3 we present the three-orbital Hubbard model (3oH) results [69] for various electron fillings. For $n = 4.5$, the atomic limit of our setup [21] predicts one Hund excitation (between states with 5 and 4 electrons) with energy $2J_H$ [70], along with several $U$-dependent Hubbard excitations. We pinpoint the Hund band using the projector analysis, shown in Fig. 3(b). We differentiate transitions arriving at $|\uparrow\downarrow,\uparrow,\uparrow\rangle$ and $|\uparrow\downarrow,\downarrow,\uparrow\rangle$. Similarly, for the $n = 3.5$ filling, the atomic limit implies Hund bands in photoemission at $3J_H$ and $5J_H$. They are shown in Fig. 3(c). The $3J_H$ band is a transition to a low-spin $S = 1/2$ state [$\mathcal{P}$ onto $|\uparrow,\downarrow,\uparrow\rangle$; see Fig. 3(a)]. The $5J_H$ band originates in states of the form $|\uparrow\downarrow,0,\uparrow\rangle \pm |0,\uparrow\downarrow,\uparrow\rangle$, where "$-$" is degenerate with the $3J_H$ excitation while "$+$" forms the $5J_H$ peak. The latter are the holon-doublon states [34–39]. Their origin was discussed in [34,36] but without realizing they are a particular example of the generic physics of Hund bands revealed here. Surprisingly, the $2J_H$ band persists even for $n = 3.5$ (as implied by the smaller but nonvanishing weight of $|\uparrow\downarrow,\downarrow,\uparrow\rangle$), inducing a third Hund peak, absent in the atomic spectrum. The intensity of this mode decreases with $U$.

By contrast, for *integer* filling $n \in \{1, 2, 3, \ldots\}$, the atomic limit alone does not predict the Hund bands. The atom lacks the necessary charge fluctuations as its gs does not span adjacent particle-number subspaces. Thus, only the "standard" Hubbard bands should be observed [5,71]. However, in the lattice, the charge fluctuations are possible provided the interaction $U$ is not too large at a given filling $n$. For half filling, the fluctuations vanish already for $U \sim W$ and the Hubbard

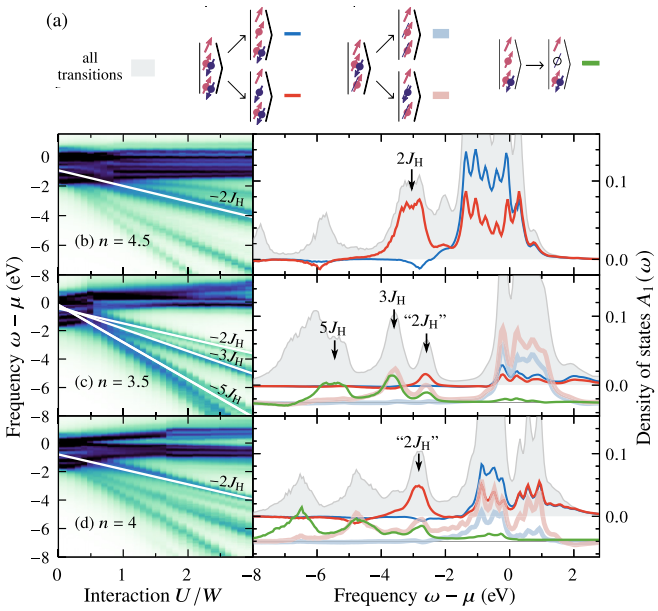


FIG. 3. (a) Sketch of the transitions to final configurations that contribute to the Hund bands of the three-orbital Hubbard model (3oH). For clarity, we present only the representative configurations (while the results are summed over several configurations of the same type). The labeling of the arrows follows Fig. 2. (b)–(d) DOS $A_1(\omega)$ of the itinerant orbital ($\gamma = 1$) of 3oH with $J_H/U = 0.25$. Left panels depict $A_1(\omega)$ as function of the interaction $U$, while right panels show detailed spectra with projections for $U/W = 2$. (b)–(d) depict results for $n = 4.5$, $n = 3.5$, and $n = 4$, respectively. The arrows on the right panels point at the Hund bands [70], with "..." denoting the peaks observable only on a lattice. The solid lines in the left column mark the $-2J_H$, $-3J_H$, and $-5J_H$ slopes. The unlabeled peaks are Hubbard bands which have a $U$ dependence [21]. Results obtained with DMRG on an $L = 8$ lattice with broadening $\eta = 0.1$.

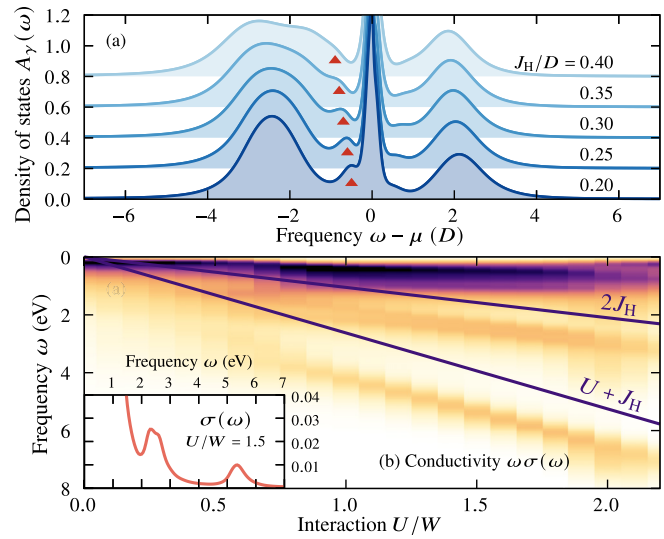


FIG. 4. (a) $A_\gamma(\omega)$ calculated with the DMFT method for an orbitally degenerate three-orbital Hubbard model with semicircular DOS, integer filling $n = 4$, $U/D = 3.8$, and $J_H/D = 0.20, \ldots, 0.40$. The half bandwidth $D = 1$ is used as the energy unit; see [21] for details. Triangles mark $\omega = -2J_H$ with a constant shift of $-0.1$ [70]. (b) Optical conductivity $\omega\sigma(\omega)$ vs the interaction $U$. The lines mark the atomic-limit energy scales. Notice the $2J_H$ peak appearing for $U/W > 0.8$. Inset: Data for $U/W = 1.5$. Results obtained via DMRG for the gKH model with $n = 1.5$, $J_H/U = 0.25$, $L = 24$ sites, and broadening $\eta = 0.1$.

bands are well developed [see, e.g., the inset of Fig. 2(a)]. Away from half filling, $U \sim W$ does not suppress the fluctuations. They are significant even at integer $n$, and vanish only at elevated $U \sim 10W$ [5,61,72]. Consequently, the many-body gs has significant contribution of states with neighboring local occupations, $|n-1\rangle$ and $|n+1\rangle$. Adding/removing particles in these states allows reaching the higher multiplets of the atomic ground-state subspace $|n\rangle$, and the Hund bands emerge.

Consider the $n = 4$ case, i.e., one electron above half filling for 3oH. In the atom, the gs has only 4-electron configurations, but in the lattice we find significant on-site fluctuations to 5- and 3-electron states [4,73]. In Fig. 3(d), we project onto the same configurations as for $n = 4.5$ and again find the $2J_H$ Hund band (originating in the $n = 5 \to 4$ transitions). We should notice only half of the peak is exhausted by the projection onto $|\uparrow\downarrow, \downarrow, \uparrow\rangle$ and our results also indicate a weak $U$ dependence. We could not discern Hund bands corresponding to electron addition processes from 3-electron states: For a high-spin initial configuration $n = 3$, $S = 3/2$, the selection rules forbid reaching the low-spin $n = 4$, $S = 0$ state [74].

*Conclusions.* We showed that the charge fluctuations and finite Hund exchange present in the multiorbital Hubbard model cause the formation of unique bands of excitations. These Hund bands are formed by the energetically costly low-angular-momentum states (i.e., on-site configurations which break the Hund's rules) and they do not depend on Hubbard $U$. The latter makes them distinct from the Hubbard-band multiplet splittings. Among the Hund bands the canonical spin-singlet mode ($\omega \simeq 2J_H$) is especially prevalent.

Our results are a generic consequence of multiorbital systems. They originate in the existence of higher multiplets; hence they do not depend on the presence of the orbital-selective Mott phase (see [21] for additional discussion) or on the system's dimensionality. To confirm this, in Fig. 4(a), we present DMFT calculations in infinite dimensions. We focus on generic rather than material-specific features and consider a semicircular density of states and orbital degeneracy [21]. The DMFT results clearly show the $2J_H$ mode. In Supplemental Material [21], we repeat the calculations for a typical $t_{2g}$ DOS and also find the Hund band.

Our findings are relevant for ARPES, resonant inelastic x-ray scattering [75], Raman spectroscopy [76,77], nonequilibrium investigations [78–80], and reflectivity/transmission measurements [81–84]. Figure 4(b) demonstrates the last: It presents how the optical conductivity [21] evolves with $U$ for the gKH model at $n = 1.5$. Crucially, we observe the Hund band at $\omega \simeq 2J_H$. Often, such additional spectral features are attributed to the interband transitions. Here, we showed that additional modes can also originate in the Hund exchange and, consequently, can be used to estimate the value of $J_H$.

*Acknowledgments.* M.Ś. and J.H. acknowledge grant support by the Polish National Agency of Academic Exchange

(NAWA) under Contract No. PPN/PPO/2018/1/00035 and by the National Science Centre (NCN), Poland, via Project No. 2019/35/B/ST3/01207. J.M. acknowledges support by the Slovenian Research Agency under Programs No. P1-0044, No. J1-2458, No. J1-2456, and No. J1-2463. G.A. was supported by the U.S. Department of Energy, Office of Science, National Quantum Information Science Research Centers, Quantum Science Center. E.D. was supported by the U.S. Department of Energy, Office of Science, Basic Energy Sciences, Materials Sciences and Engineering Division. Some of the calculations have been carried out using resources provided by the Wroclaw Centre for Networking and Supercomputing [85].

[1] D. J. Scalapino, A common thread: The pairing interaction for unconventional superconductors, Rev. Mod. Phys. **84**, 1383 (2012).

[2] E. Dagotto, Correlated electrons in high-temperature superconductors, Rev. Mod. Phys. **66**, 763 (1994).

[3] S. M. O'Mahony, W. Ren, W. Chen, Y. X. Chong, X. Liu, H. Eisaki, S. Uchida, M. H. Hamidian, and J. C. S. Davis, On the electron pairing mechanism of copper-oxide high temperature superconductivity, Proc. Natl. Acad. Sci. USA **119**, e2207449119 (2022).

[4] Z. Yin, K. Haule, and G Kotliar, Kinetic frustration and the nature of the magnetic and paramagnetic states in iron pnictides and iron chalcogenides, Nat. Mater. **10**, 932 (2011).

[5] A. Georges, L. Medici, and J. Mravlje, Strong correlations from Hund's coupling, Annu. Rev. Condens. Matter Phys. **4**, 137 (2013).

[6] M. Yi, Y. Zhang, Z.-X. Shen, and D. Lu, Role of the orbital degree of freedom in iron-based superconductors, npj Quantum Mater. **2**, 57 (2017).

[7] A. Koga, N. Kawakami, T. M. Rice, and M. Sigrist, Orbital-Selective Mott Transitions in the Degenerate Hubbard Model, Phys. Rev. Lett. **92**, 216402 (2004).

[8] L. de'Medici, A. Georges, and S. Biermann, Orbital-selective Mott transition in multiband systems: Slave-spin representation and dynamical mean-field theory, Phys. Rev. B **72**, 205124 (2005).

[9] J. Rincón, A. Moreo, G. Alvarez, and E. Dagotto, Exotic Magnetic Order in the Orbital-Selective Mott Regime of Multiorbital Systems, Phys. Rev. Lett. **112**, 106405 (2014).

[10] J. Herbrych, J. Heverhagen, N. D. Patel, G. Alvarez, M. Daghofer, A. Moreo, and E. Dagotto, Novel Magnetic Block States in Low-Dimensional Iron-Based Superconductors, Phys. Rev. Lett. **123**, 027203 (2019).

[11] A. Damascelli, Z. Hussain, and Z.-X. Shen, Angle-resolved photoemission studies of the cuprate superconductors, Rev. Mod. Phys. **75**, 473 (2003).

[12] Y. Wang, Y. He, K. Wohlfeld, M. Hashimoto, E. W. Huang, D. Lu, S.-K. Mo, S. Komiya, C. Jia, B. Moritz, Z.-X. Shen, and T. P. Devereaux, Emergence of quasiparticles in a doped Mott insulator, Commun. Phys. **3**, 210 (2020).

[13] H. Benthien, F. Gebhard, and E. Jeckelmann, Spectral Function of the One-Dimensional Hubbard Model away from Half Filling, Phys. Rev. Lett. **92**, 256401 (2004).

[14] A. E. Feiguin and G. A. Fiete, Spin-Incoherent Behavior in the Ground State of Strongly Correlated Systems, Phys. Rev. Lett. **106**, 146401 (2011).

[15] F. Essler, H. Frahm, F. Göhmann, A. Klümper, and V. E. Korepin, *The One-Dimensional Hubbard Model* (Cambridge University Press, Cambridge, 2010).

[16] A. Georges, G. Kotliar, W. Krauth, and M. J. Rozenberg, Dynamical mean-field theory of strongly correlated fermion systems and the limit of infinite dimensions, Rev. Mod. Phys. **68**, 13 (1996).

[17] E. Jakobi, N. Blümer, and P. van Dongen, Orbital-selective Mott transitions in a doped two-band Hubbard model with crystal field splitting, Phys. Rev. B **87**, 205135 (2013).

[18] A. van Roekeghem, P. Richard, H. Ding, and S. Biermann, Spectral properties of transition metal pnictides and chalcogenides: Angle-resolved photoemission spectroscopy and dynamical mean-field theory, C. R. Phys. **17**, 140 (2016).

[19] A. Tamai, M. Zingl, E. Rozbicki, E. Cappelli, S. Riccò, A. de la Torre, S. McKeown Walker, F. Y. Bruno, P. D. C. King, W. Meevasana, M. Shi, M. Radović, N. C. Plumb, A. S. Gibbs, A. P. Mackenzie, C. Berthod, H. U. R. Strand, M. Kim, A. Georges, and F. Baumberger, High-Resolution Photoemission on $Sr_2RuO_4$ Reveals Correlation-Enhanced Effective Spin-Orbit Coupling and Dominantly Local Self-Energies, Phys. Rev. X **9**, 021048 (2019).

[20] D. Bauernfeind, M. Zingl, R. Triebl, M. Aichhorn, and H. G. Evertz, Fork Tensor-Product States: Efficient Multiorbital Real-Time DMFT Solver, Phys. Rev. X **7**, 031013 (2017).

[21] See Supplemental Material at http://link.aps.org/supplemental/10.1103/PhysRevB.108.L081102 for (1) Refs. [22–30], not cited in the main text, (2) definition of the single-particle spectral function, (3) three-orbital results for the momentum dependence of the spectral function, (4) two- and three-orbital results for fixed $J_H$ (showing that Hund bands are $U$ independent whereas Hubbard bands are not), (5) derivation of the atomic-limit energies for the three-orbital model, (6) Hund bands in an orbitally degenerate three-orbital system, (7) Hund bands for orbital-dependent interactions, (8) details of the DMFT calculations, (9) DMFT calculations for a realistic $t_{2g}$ density of states, and (10) definition of the optical conductivity $\sigma(\omega)$.

[22] E. Jeckelmann, Dynamical density-matrix renormalization-group method, Phys. Rev. B **66**, 045114 (2002).

[23] W. Stephan and K. Penc, Dynamical density-density correlations in one-dimensional Mott insulators, Phys. Rev. B **54**, R17269 (1996).

[24] R. Žitko and T. Pruschke, Energy resolution and discretization artifacts in the numerical renormalization group, Phys. Rev. B **79**, 085106 (2009).

[25] R. Žitko, NRG Ljubljana, https://zenodo.org/record/4841076

[26] H. Wadati, J. Mravlje, K. Yoshimatsu, H. Kumigashira, M. Oshima, T. Sugiyama, E. Ikenaga, A. Fujimori, A. Georges, A. Radetinac, K. S. Takahashi, M. Kawasaki, and Y. Tokura, Photoemission and DMFT study of electronic correlations in

$SrMoO_3$: Effects of Hund's rule coupling and possible plasmonic sideband, Phys. Rev. B **90**, 205131 (2014).

[27] D. Stricker, J. Mravlje, C. Berthod, R. Fittipaldi, A. Vecchione, A. Georges, and D. van der Marel, Optical Response of $Sr_2RuO_4$ Reveals Universal Fermi-Liquid Scaling and Quasiparticles beyond Landau Theory, Phys. Rev. Lett. **113**, 087404 (2014).

[28] K. M. Stadler, Z. P. Yin, J. von Delft, G. Kotliar, and A. Weichselbaum, Dynamical Mean-Field Theory Plus Numerical Renormalization-Group Study of Spin-Orbital Separation in a Three-Band Hund Metal, Phys. Rev. Lett. **115**, 136401 (2015).

[29] A. Horvat, R. Žitko, and J. Mravlje, Non-Fermi-liquid fixed point in multi-orbital Kondo impurity model relevant for Hund's metals, arXiv:1907.07100.

[30] E. Walter, K. M. Stadler, S. S. B. Lee, Y. Wang, G. Kotliar, A. Weichselbaum, and J. von Delft, Uncovering Non-Fermi-Liquid Behavior in Hund Metals: Conformal Field Theory Analysis of an SU(2) × SU(3) Spin-Orbital Kondo Model, Phys. Rev. X **10**, 031052 (2020).

[31] K. Hallberg, D. J. García, P. S. Cornaglia, J. I. Facio, and Y. Núñez-Fernández, State-of-the-art techniques for calculating spectral functions in models for correlated materials, Europhys. Lett. **112**, 17001 (2015).

[32] K. M. Stadler, G. Kotliar, A. Weichselbaum, and J. von Delft, Hundness versus Mottness in a three-band Hubbard-Hund model: On the origin of strong correlations in Hund metals, Ann. Phys. **405**, 365 (2019).

[33] D. Sutter, C. G. Fatuzzo, S. Moser, M. Kim, R. Fittipaldi, A. Vecchione, V. Granata, Y. Sassa, F. Cossalter, G. Gatti, M. Grioni, H. M. Rønnow, N. C. Plumb, C. E. Matt, M. Shi, M. Hoesch, T. K. Kim, T.-R. Chang, H.-T. Jeng, C. Jozwiak *et al.*, Hallmarks of Hunds coupling in the Mott insulator $Ca_2RuO_4$, Nat. Commun. **8**, 15176 (2017).

[34] Y. Núñez-Fernández, G. Kotliar, and K. Hallberg, Emergent low-energy bound states in the two-orbital Hubbard model, Phys. Rev. B **97**, 121113(R) (2018).

[35] Y. Niu, J. Sun, Y. Ni, J. Liu, Y. Song, and S. Feng, Doublon-holon excitations split by Hund's rule coupling within the orbital-selective Mott phase, Phys. Rev. B **100**, 075158 (2019).

[36] F. B. Kugler, S.-S. B. Lee, A. Weichselbaum, G. Kotliar, and J. von Delft, Orbital differentiation in Hund metals, Phys. Rev. B **100**, 115159 (2019).

[37] Y. Komijani, K. Hallberg, and G. Kotliar, Renormalized dispersing multiplets in the spectrum of nearly Mott localized systems, Phys. Rev. B **99**, 125150 (2019).

[38] K. Hallberg and Y. Núñez-Fernández, Subbands in the doped two-orbital Kanamori-Hubbard model, Phys. Rev. B **102**, 245138 (2020).

[39] N. Aucar Boidi, H. Fernández García, Y. Núñez Fernández, and K. Hallberg, In-gap band in the one-dimensional two-orbital Kanamori-Hubbard model with interorbital Coulomb interaction, Phys. Rev. Res. **3**, 043213 (2021).

[40] A. Richaud, M. Ferraretto, and M. Capone, Interaction-resistant metals in multicomponent Fermi systems, Phys. Rev. B **103**, 205132 (2021).

[41] S. R. White, Density Matrix Formulation for Quantum Renormalization Groups, Phys. Rev. Lett. **69**, 2863 (1992).

[42] U. Schollwöck, The density-matrix renormalization group, Rev. Mod. Phys. **77**, 259 (2005).

[43] S. R. White, Density matrix renormalization group algorithms with a single center site, Phys. Rev. B **72**, 180403(R) (2005).

[44] G. Alvarez, The density matrix renormalization group for strongly correlated electron systems: A generic implementation, Comput. Phys. Commun. **180**, 1572 (2009).

[45] A. Nocera and G. Alvarez, Spectral functions with the density matrix renormalization group: Krylov-space approach for correction vectors, Phys. Rev. E **94**, 053308 (2016).

[46] We use the DMRG++ computer program developed at Oak Ridge National Laboratory (see https://g1257.github.io/dmrgPlusPlus). We run DMRG within the single-center site approach and keep up to $M = 1200$ states during ∼11 finite-size sweeps. The truncation error for the ground state is $\lesssim 10^{-6}$. The spectral functions are calculated directly in frequency space using the Krylov-space approach for correction vectors. For the calculation of the optical conductivity $\sigma(\omega)$, we use up to $M = 2000$ states during 15 sweeps.

[47] P. Prelovšek and J. Bonča, Ground state and finite temperature Lanczos methods, in *Strongly Correlated Systems—Numerical Methods*, edited by A. Avella and F. Mancini (Springer, Berlin, 2013).

[48] M. D. Watson, S. Backes, A. A. Haghighirad, M. Hoesch, T. K. Kim, A. I. Coldea, and R. Valentí, Formation of Hubbard-like bands as a fingerprint of strong electron-electron interactions in FeSe, Phys. Rev. B **95**, 081106(R) (2017).

[49] D. V. Evtushinsky, M. Aichhorn, Y. Sassa, Z.-H. Liu, J. Maletz, T. Wolf, A. N. Yaresko, S. Biermann, S. V. Borisenko, and B. Büchner, Direct observation of dispersive lower Hubbard band in iron-based superconductor FeSe, arXiv:1612.02313.

[50] T. Hotta and E. Dagotto, Prediction of Orbital Ordering in Single-Layered Ruthenates, Phys. Rev. Lett. **88**, 017201 (2001).

[51] D. Sutter, M. Kim, C. E. Matt, M. Horio, R. Fittipaldi, A. Vecchione, V. Granata, K. Hauser, Y. Sassa, G. Gatti, M. Grioni, M. Hoesch, T. K. Kim, E. Rienks, N. C. Plumb, M. Shi, T. Neupert, A. Georges, and J. Chang, Orbitally selective breakdown of Fermi liquid quasiparticles in $Ca_{1.8}Sr_{0.2}RuO_4$, Phys. Rev. B **99**, 121115(R) (2019).

[52] H. Gretarsson, H. Suzuki, H. Kim, K. Ueda, M. Krautloher, B. J. Kim, H. Yavaş, G. Khaliullin, and B. Keimer, Observation of spin-orbit excitations and Hund's multiplets in $Ca_2RuO_4$, Phys. Rev. B **100**, 045123 (2019).

[53] B. Yuan, J. P. Clancy, A. M. Cook, C. M. Thompson, J. Greedan, G. Cao, B. C. Jeon, T. W. Noh, M. H. Upton, D. Casa, T. Gog, A. Paramekanti, and Young-June Kim, Determination of Hund's coupling in 5*d* oxides using resonant inelastic x-ray scattering, Phys. Rev. B **95**, 235114 (2017).

[54] E. M. Pärschke and R. Ray, Influence of the multiplet structure on the photoemission spectra of spin-orbit driven Mott insulators: Application to $Sr_2IrO_4$, Phys. Rev. B **98**, 064422 (2018).

[55] V. I. Anisimov, D. Bukhvalov, and T. M. Rice, Electronic structure of possible nickelate analogs to the cuprates, Phys. Rev. B **59**, 7901 (1999).

[56] J. Zhang, A. S. Botana, J. W. Freeland, D. Phelan, H. Zheng, V. Pardo, M. R. Norman, and J. F. Mitchell, Large orbital polarization in a metallic square-planar nickelate, Nat. Phys. **13**, 864 (2017).

[57] D. Li, K. Lee, B. Y. Wang, M. Osada, S. Crossley, H. R. Lee, Y. Cui, Y. Hikita, and H. Y. Hwang, Superconductiv-

ity in an infinite-layer nickelate, Nature (London) **572**, 624 (2019).

[58] X. Wan, V. Ivanov, G. Resta, I. Leonov, and S. Y. Savrasov, Exchange interactions and sensitivity of the Ni two-hole spin state to Hund's coupling in doped $NdNiO_2$, Phys. Rev. B **103**, 075123 (2021).

[59] Q. Gu. and H.-H. Wen., Superconductivity in nickel-based 112 systems, Innovation **3**, 100202 (2021).

[60] J. Herbrych, N. Kaushal, A. Nocera, G. Alvarez, A. Moreo, and E. Dagotto, Spin dynamics of the block orbital-selective Mott phase, Nat. Commun. **9**, 3736 (2018).

[61] J. Rincón, A. Moreo, G. Alvarez, and E. Dagotto, Quantum phase transition between orbital-selective Mott states in Hund's metals, Phys. Rev. B **90**, 241105(R) (2014).

[62] M. Środa, E. Dagotto, and J. Herbrych, Quantum magnetism of iron-based ladders: Blocks, spirals, and spin flux, Phys. Rev. B **104**, 045128 (2021).

[63] J. Herbrych, G. Alvarez, A. Moreo, and E. Dagotto, Block orbital-selective Mott insulators: A spin excitation analysis, Phys. Rev. B **102**, 115134 (2020).

[64] For the three-orbital model, the actual kinetic-energy span equals 2.45 eV. However, we use $W = 2.1$ eV as the energy unit. This facilitates easier comparison with other models.

[65] M. Mourigal, S. Wu, M. B. Stone, J. R. Neilson, J. M. Caron, T. M. McQueen, and C. L. Broholm, Block Magnetic Excitations in the Orbitally Selective Mott Insulator $BaFe_2Se_3$, Phys. Rev. Lett. **115**, 047401 (2015).

[66] Y. Nambu, K. Ohgushi, S. Suzuki, F. Du, M. Avdeev, Y. Uwatoko, K. Munakata, H. Fukazawa, S. Chi, Y. Ueda, and T. J. Sato, Block magnetism coupled with local distortion in the iron-based spin-ladder compound $BaFe_2Se_3$, Phys. Rev. B **85**, 064413 (2012).

[67] S. Wu, J. Yin, T. Smart, A. Acharya, C. L. Bull, N. P. Funnell, T. R. Forrest, G. Simutis, R. Khasanov, S. K. Lewin, M. Wang, B. A. Frandsen, R. Jeanloz, and R. J. Birgeneau, Robust block magnetism in the spin ladder compound $BaFe_2Se_3$ under hydrostatic pressure, Phys. Rev. B **100**, 214511 (2019).

[68] N. D. Patel, A. Nocera, G. Alvarez, A. Moreo, S. Johnston, and E. Dagotto, Fingerprints of an orbital-selective Mott phase in the block magnetic state of $BaFe_2Se_3$ ladders, Commun. Phys. **2**, 64 (2019).

[69] For our parameters, the three-orbital model is in the OSMP (with $\gamma = 2$ localized) for $U/W \gtrsim 0.9$.

[70] We mark each Hund band by its $J_H$ dependence. The $J_H$ dependence agrees between the lattice and the atom very well, even though the exact values of the excitation energies may differ. Such a situation is clearly observed in Fig. 2(a). In subsequent figures, we often shift the atomic energy scales by a constant so as to match the evolution of the lattice peaks.

[71] L. de' Medici, J. Mravlje, and A. Georges, Janus-Faced Influence of Hund's Rule Coupling in Strongly Correlated Materials, Phys. Rev. Lett. **107**, 256401 (2011).

[72] K. Haule and G. Kotliar, Coherence-incoherence crossover in the normal state of iron oxypnictides and importance of Hund's rule coupling, New J. Phys. **11**, 025021 (2009).

[73] J. Karp, M. Bramberger, M. Grundner, U. Schollwöck, A. J. Millis, and M. Zingl, $Sr_2MoO_4$ and $Sr_2RuO_4$: Disentangling the Roles of Hund's and van Hove Physics, Phys. Rev. Lett. **125**, 166401 (2020).

[74] The same selection rules apply at $n = 3.5$, where the $2J_H$ and $5J_H$ Hund bands of $n = 4$ subspace are not observed in electron addition processes (i.e., above $\mu$).

[75] P. Werner, S. Johnston, and M. Eckstein, Nonequilibrium-DMFT based RIXS investigation of the two-orbital Hubbard model, Europhys. Lett. **133**, 57005 (2021).

[76] T. Tohyama, J. Inoue, and S. Maekawa, Raman scattering in the two-dimensional Hubbard model, Physica B: Condens. Matter **186**, 968 (1992).

[77] H.-Y. Lu, D. Wang, S. Chen, W. Wang, and P.-F. Gong, Electronic Raman spectra in iron-based superconductors with two-orbital model, Physica C: Supercond. **471**, 453 (2011).

[78] H. U. R. Strand, D. Golež, M. Eckstein, and P. Werner, Hund's coupling driven photocarrier relaxation in the two-band Mott insulator, Phys. Rev. B **96**, 165104 (2017).

[79] F. Petocchi, S. Beck, C. Ederer, and P. Werner, Hund excitations and the efficiency of Mott solar cells, Phys. Rev. B **100**, 075147 (2019).

[80] K. Gillmeister, D. Golež, C.-T. Chiang, N. Bittner, Y. Pavlyukh, J. Berakdar, P. Werner, and W. Widdra, Ultrafast coupled charge and spin dynamics in strongly correlated NiO, Nat. Commun. **11**, 4095 (2020).

[81] A. A. Schafgans, S. J. Moon, B. C. Pursley, A. D. LaForge, M. M. Qazilbash, A. S. Sefat, D. Mandrus, K. Haule, G. Kotliar, and D. N. Basov, Electronic Correlations and Unconventional Spectral Weight Transfer in the High-Temperature Pnictide $BaFe_{2-x}Co_xAs_2$ Superconductor Using Infrared Spectroscopy, Phys. Rev. Lett. **108**, 147002 (2012).

[82] A. Charnukha, Optical conductivity of iron-based superconductors, J. Phys.: Condens. Matter **26**, 253203 (2014).

[83] M. Nakajima, K. Yanase, F. Nabeshima, Y. Imai, A. Maeda, and S. Tajima, Gradual Fermi-surface modification in orbitally ordered state of FeSe revealed by optical spectroscopy, Phys. Rev. B **95**, 184502 (2017).

[84] A. Pal, M. Chinotti, J.-H. Chu, H.-H. Kuo, I. R. Fisher, and L. Degiorgi, Optical conductivity of iron-based superconductors, npj Quantum Mater. **4**, 3 (2019).

[85] See http://wcss.pl